Numerical Modeling of Microdrop Motion in a Digital Microfluidic Multiplexer

A. Ahmadi*, H. Najjaran*, J. F. Holzman*, M. Hoorfar*
*School of Engineering, University of British Columbia Okanagan,
Kelowna, British Columbia, Canada, V1V 1V7

ABSTRACT

This paper introduces a computationally efficient numerical modeling approach for microdroplet motion within a new Digital Microfluidic Multiplexer structure. This structure offers an enhanced level of controllability and flexibility in drop actuation compared to the existing digital microfluidic systems that rely on addressable (square-matrix) cell structures. The real-time control of microdroplets under the resulting electrical, magnetic and hydrodynamic effects requires a reliable and computationally efficient model of the micron-scale kinematic forces. The proposed numerical model analyzes the time-variant average microdrop velocity using a computational-fluid-dynamic (CFD) code that solves the Navier-Stokes equation for velocity and pressure distributions inside the microdroplet. The estimated average velocity is modified according to the contact-angle hysteresis and an external force (e.g., induced by a magnetic field) using an iterative method.

Keywords: Digital Microfluidic Multiplexer, CFD, Microdroplet, Modeling, Hysteresis

1 INTRODUCTION

The development of micron-scale devices has evolved through a technological trend in the recent decades. This trend started in the microelectronics industry and quickly spread to many new fields, including fluid mechanics and integrated digital microfluidics. With digital microfluidic systems, discrete droplets can be manipulated as an alternative approach to overcome the challenges of continuous flow systems. In contrast to continuous flow, droplet-based systems are compatible with wall-less structures, and droplet manipulation can be carried out on the surface of a planar substrate in a reconfigurable and scalable manner. They can be used as programmable "microfluidic processors" in bio-related areas such as parallel DNA analysis, real-time biomolecular detection and automated drug discovery [1].

Modeling of droplet motion is very important in designing and controlling digital microfluidic systems, and most recent efforts have focused on predicting the bulk velocity of droplets on the chips. While the average velocity of these droplets is important, it has been shown that the internal motion of the droplet can also directly affect the droplet behavior [2]. In most previous studies, one dimensional flow has been assumed for the internal flow, and the vertical component of velocity inside the droplet has been ignored. Beni and Tenan [3], for example, used the Poiseuille flow assumption for flow inside the droplet [3], while Nichols et al. [4] included the effects of an external force on the droplet motion. In the latter, the system was analyzed analytically with the Navier-Stokes equation by neglecting the vertical component of the velocity inside the droplet. In a recent study by Walker and Shapiro [5], a two dimensional three-phase contact line motion is modeled assuming one dimensional Hele-Shaw flow inside the drop.

When the height of the channel is much smaller than the radius of the investigated droplet, an assumption of one dimensional flow inside the drop may lead to a good approximation for the bulk velocity of the drop. However, when the height of the channel is comparable to the radius of the drop, the vertical component of the velocity inside the droplet plays an important role in drop dynamics as the fluid flow becomes two dimensional in nature. Two-dimensional flow strongly affects the bulk pressure distribution, i.e., the vertical component of the pressure gradient at the interfaces, and the ultimate bulk microdrop velocity. Unlike the previous models of drop motion based upon the Poiseuille flow pressure distribution assumption [2, 3, 4], the present work models a micron-scale integrated microfluidic structure with the two dimensional Navier-Stokes equation. External body forces and hysteresis effects are included in the numerical model, and the results are applied to the analysis of the proposed Digital Microfluidic Multiplexer structure. It has been shown that the resulting two-dimensional fluid dynamics dominates the operation of digital microfluidic devices in the investigated micron-sized dimensions, and cannot be ignored.

2 METHODOLOGY

2.1 Description of the Device

A schematic of a Digital Microfluidic Multiplexer device is shown in Figure 1. Localized electrical current are induced in the Digital Microfluidic Multiplexer structure through the application of voltage differences between perpendicular x- and z- addressable electrodes. Regions with identical x- and z-electrode voltages (identically-biased) have no net current whereas regions with differently-biased electrodes will have net current flow from the positive electrode to the negative electrode. Such an arrangement avoids the complexities of integrated address lines in square-matrix cell structures and multi-

dimensional via-lines when large numbers of electrodes with particularly small dimensions are desired. Ultimately, an external body force is applied using an external electric field, and the net motion of the microdrop is dictated by balancing this magnetic force and the internal capillary forces.

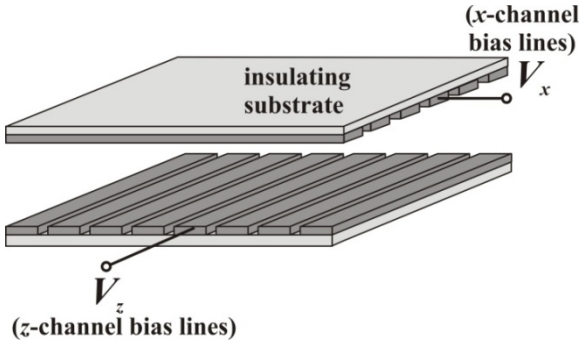

Figure 1: The Digital Microfluidic Multiplexer. The conductive *x*-channel and *z*-channel bias lines are used to control the motion of the microfluidic drop within the central fluid control layer [4].

2.2 Governing Equations

With the micron-sized dimensions of the Digital Microfluidic Multiplexer in mind, the main focus of the present work will be on the effects of internal fluid motion inside droplets. The deformation of droplet boundary will not be studied here, and a cylindrical shape will be assumed for the droplet (Figure 2). In this way, the three-dimensional motion of the system can be approximated by a two-dimensional flow within a cross-sectional meridian plane. This assumption is valid for large body forces in the x direction where the flow in the z direction can be neglected (Figure 2).

The analysis begins through the dimensionless Navier-Stokes equations:

$$\frac{\partial P^*}{\partial t^*}+\frac{\partial u^*}{\partial x^*}+\frac{\partial v^*}{\partial y^*}=0 \tag{1}$$

$$\frac{\partial u^*}{\partial t^*}+\frac{\partial u^{*2}}{\partial x^*}+\frac{\partial u^* v^*}{\partial y^*}=-\frac{\partial P^*}{\partial x^*}+\frac{1}{\mathrm{Re}}\left(\frac{\partial^2 u^*}{\partial x^{*2}}+\frac{\partial^2 u^*}{\partial y^{*2}}\right)+F_x^* \tag{2}$$

$$\frac{\partial v^*}{\partial t^*}+\frac{\partial u^* v^*}{\partial x^*}+\frac{\partial v^{*2}}{\partial y^*}=-\frac{\partial P^*}{\partial y^*}+\frac{1}{\mathrm{Re}}\left(\frac{\partial^2 v^*}{\partial x^{*2}}+\frac{\partial^2 v^*}{\partial y^{*2}}\right)+F_y^* \tag{3}$$

where asterisk parameters are the dimensionless quantities ($t^*=tU_\infty/L$, $P^*=P/\left(\rho U_\infty^2\right)$, $u^*=u/U_\infty$, $v^*=v/U_\infty$ $x^*=x/L$, and $y^*=y/L$). Here, U_∞ is the reference velocity equal to the bulk droplet velocity, and L is the reference length in the problem (which is in our case equal to the height of the channel, *H*). The Reynolds number is defined as $\mathrm{Re}=U_\infty L/\nu$, where ν is the kinematic viscosity of the liquid. The term F^* is the dimensionless body force in each direction as defined by $F^*=F_b L/\left(V\rho U_\infty^2\right)$, where F_b represents the body force in the problem and V is the volume of the droplet.

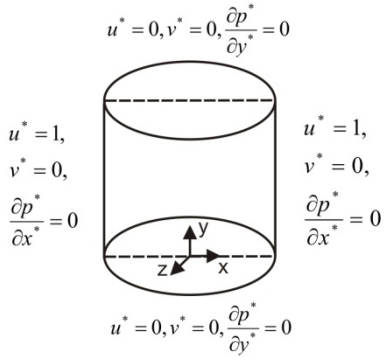

Figure 2: Boundary conditions in the meridian plane

2.3 Boundary Conditions

Boundary conditions for the two-dimensional domain are particularly important. The fluid motion inside the drop is considered with respect to a moving coordinate frame, which is attached to the droplet. In this coordinate frame, the left and right walls will be stationary (since they move with the droplet), and the top and bottom walls will have the bulk velocity of the drop. The hysteresis effect and the resulting pressure distribution in such a system are particularly important (see the following sections). Although considering a moving coordinate system may lead to a correct velocity distribution, the actual pressure distribution cannot be accurately calculated as the Euler equation, relating the pressure field to velocity field, cannot be used in viscous flows. The actual boundary conditions for the meridian plane are shown in Figure 2, and the explanation of Neumann boundary conditions for a given pressure distribution is explained in [6].

2.4 Hysteresis Effect

It is noted that all the cells around a droplet have the same voltage so that the driving force (e.g., induced by an applied magnetic field) is a body force and not of the electrowetting type. Such a body force will cause contact angle hysteresis (i.e. a difference between advancing and receding contact angles) along the three phase contact lines. It is well understood that the interfacial properties is related to the pressure difference across the liquid-vapor interface based on the Laplace equation of the capillarity [3]. Such a condition gives

$$P_A-P_R=\frac{2}{h}\bar{\gamma}, \tag{4}$$

where $\bar{\gamma}$ represents the total friction on the drop. A linear dependence of $\bar{\gamma}$ on $\bar{u}$ is assumed here [3] giving

$$\bar{\gamma}=\alpha+\beta\bar{u}, \tag{5}$$

NSTI-Nanotech 2008, www.nsti.org, ISBN 978-1-4200-8505-1 Vol. 3

where α and β represent the static and dynamic friction coefficients, respectively. The value of β is 0.1 Pa·s [7]), and a sufficiently small $\alpha \approx 0$ value is assumed for the static friction where a study of different values of α can be found in [4].

Equation (4) relates the pressure difference of the advancing and receding edges of the droplet to the afore-mentioned hysteresis effect. This hysteresis effect is included in the CFD code in such a way that the pressure distribution is corrected at each step. The numerical routine starts with an initial average velocity which is based on the analytical solution of the Navier-Stokes equation (by ignoring the vertical component of the velocity), and this initial average velocity is used for calculating our dimensionless parameters. An iterative approach is then used to solve for the flow dynamics inside the droplet, and the resulting velocity distribution yields the ultimate droplet average velocity. This algorithm is shown in Figure 3. The trend of convergence is also shown in Figure 4. The average velocity oscillates between two values; the upper one is the value obtained based on zero vertical velocity and the lower one is for ignoring hysteresis effect.

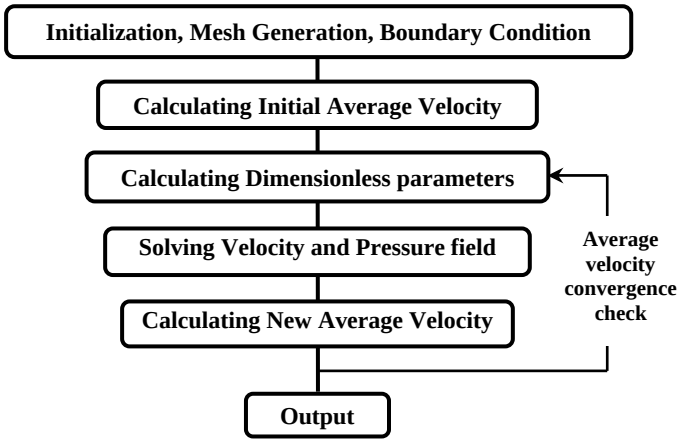

Figure 3: Flowchart of the numerical scheme

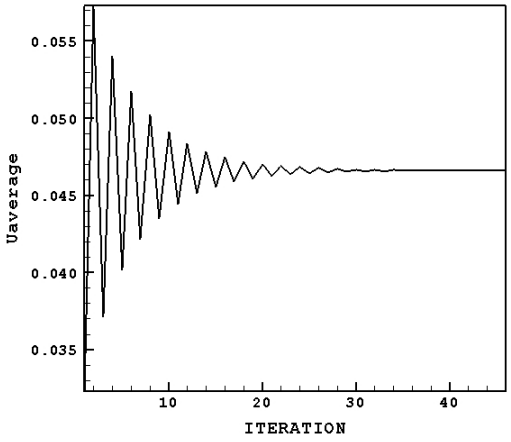

Figure 4: Trend of convergence

3 RESULTS

The no slip condition applied along the walls is apparent in the velocity field shown in Figure 4. It is observed that the stream lines align themselves to satisfy this boundary condition. The displacement of stream lines from their parallel state depends on the kinematic properties of the flow.

The bulk velocity of the droplet can be subtracted from the horizontal component of the absolute velocity to provide insight into the fluid motion inside the droplet (see Figure 5). For this purpose, a moving coordinate frame is considered that travels with the drop. It is apparent that the viscous effects lead to the formation of vortices inside the droplet. The position and strength of these vortices strongly depends on the Reynolds number as well as the applied voltage. It should be noted that most solutions for predicting the flow behavior inside droplets are based on assumptions that ignore the vertical velocity component. The vortices of Figure 5 and the vertical component shown explicitly in Figure 6 demonstrate that such a condition does not hold in these small-scale regimes. The vertical component of the velocity should not be ignored, as it becomes significantly pronounced near the drop corners.

In an effort to investigate the mass conservation inside the drop, the horizontal dimensionless velocity profile for different cross sections inside the droplet is shown in Figure 8. It is observed that the difference between the maximum velocity and average velocity increases drastically along the drop. At the liquid-vapor interface, this difference is zero and at the centre line it reaches its maximum. As it is shown in Figure 9, it is evident that the vertical component of pressure gradient cannot be ignored. As the height of the channel increases, the change in pressure across the channel becomes increasingly important since dimensionless pressure on the centerline increases along the droplet. This is due to the effect of the external body force which compensates the pressure loss due to the viscous shear stress.

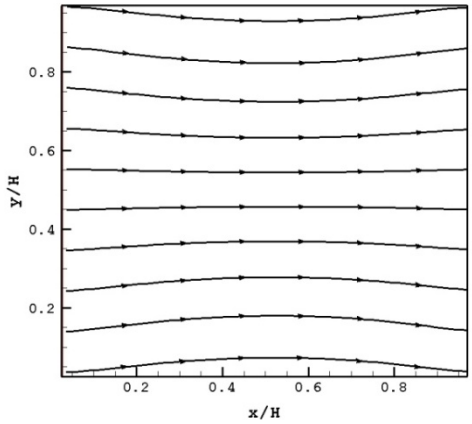

Figure 5: Absolute velocity field as a function of the normalized y/H and x/H

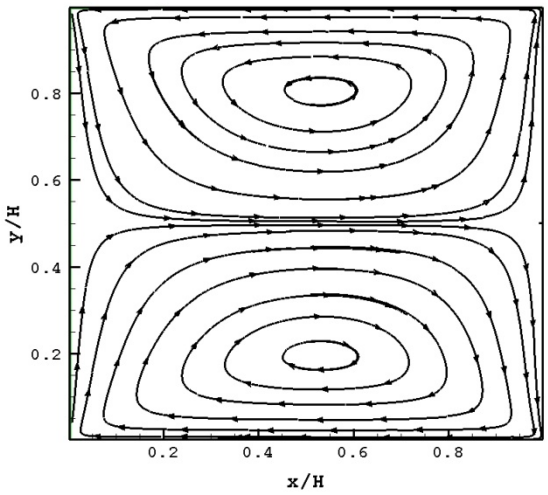

Figure 6: Internal motion of fluid inside the droplet

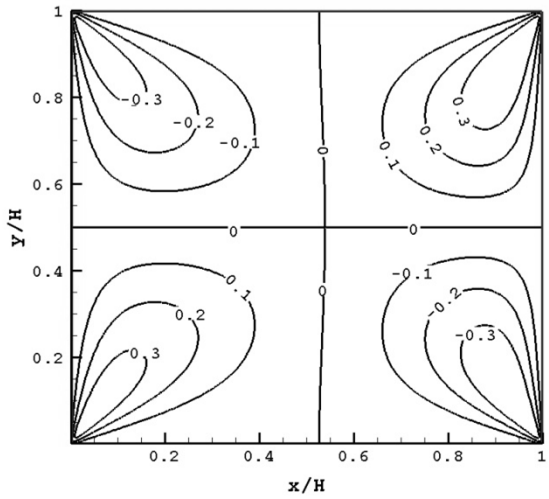

Figure 7: Horizontal dimensionless absolute velocity profile for different cross sections

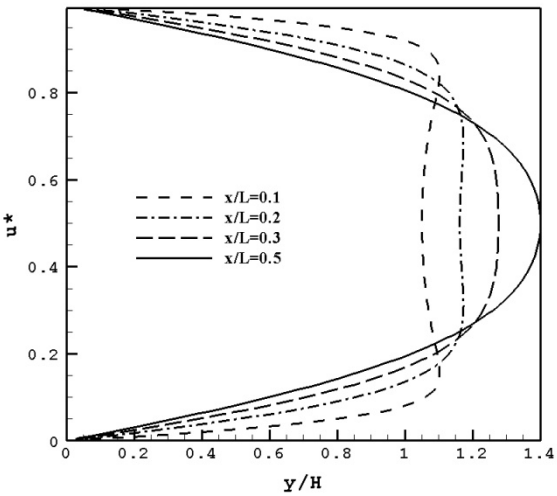

Figure 8: Dimensionless pressure distribution at the advancing cross section of the droplet

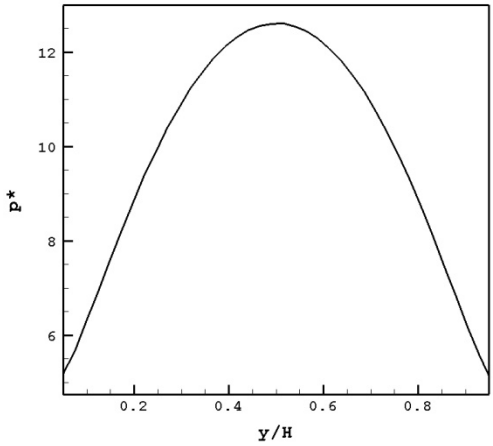

Figure 9: Vertical component of the absolute dimensionless velocity

4 SUMMARY

The effects of fluid motion inside the droplet have been studied. It is shown that vertical component of the velocity inside the droplet cannot be ignored. Moreover, it is shown that, in spite of conventional assumptions considered for solving motion of fluid inside the capillary tube, the vertical component of pressure gradient cannot be ignored. This new pressure distribution directly affects the estimated bulk velocity of the drop. The effects of body forces on drop motion have been studied, and it has been found that the body force increases the pressure along the channel.

REFERENCES

[1] K. Chakrabarty, F. Su, "Digital Microfluidic Biochips, Synthesis, Testing and Reconfiguration Techniques," CRC press, Taylor & Francis Group, 2007.

[2] J. Berthier, "Microdrops and Digital Microfluidics," William Andrew, 2008.

[3] G. Beni, M. A. Tenan, "Dynamics of Electrowetting Displays," J. Applied Physics, Vol. 52, pp. 6011-6015, 1981.

[4] J. Nichols, A. Ahmadi, M. Hoorfar, H. Najjaran, J. F. Holzman, "Micro-Drop Actuation Using Multiplexer Structures," Submitted to ICNMM 2008.

[5] S. W. Walker, B. Shapiro, "Modeling the Fluid Dynamics of Electrowetting on Dielectric (EWOD)," J. Microelectromechanical Systems, Vol. 15, No. 4, 2006.

[6] H. Lomax, T. H. Pulliam and D. W. Zingg, "Fundamentals of Computational Fluid Dynamics", Springer-Verlag, Berlin, 2001.

[7] A. M. Gaudin, A. F. Witt, "Hysteresis of Contact Angles in the System Mercury-Benzene-Water", in: Contact angle: wettability and adhesion, edited by R. F. Gould, Vol. 43, pp. 202–210, 1964.